Cancer Biol Med 2026. doi: 10.20892/j.issn.2095-3941.2025.0652

ORIGINAL ARTICLE

Bifidobacterium animalis suppresses melanoma progression and activates anti-tumor immunity by inhibiting YAP1 expression in CD8$^+$ T cells

Chengyi Li[1,2]*, Xuehua Zhang[3]*, Yichen Yang[4]*, Haotian Zeng[1,2]*, Yanqiang Shi[1,2], Jinjin Zhang[1,2], Lingjun Liu[1,2], Chenwei Zhu[1,2], Zhiwen Zhang[1,2], Chao Li[1,2], Xudong Wang[5], Xiaowu Bai[3], Haijun Deng[3], Qing Li[1,2]

[1]Dermatology Hospital, Southern Medical University, Guangzhou 510515, China; [2]The First School of Clinical Medicine, Southern Medical University, Guangzhou 510515, China; [3]Department of General Surgery, Nanfang Hospital, Southern Medical University, Guangzhou 510515, China; [4]Department of Anaesthesia and Intensive Care and Peter Hung Pain Research Institute, The Chinese University of Hong Kong, Hong Kong SAR, China; [5]State Key Laboratory of Applied Microbiology Southern China, Institute of Microbiology, Guangdong Academy of Sciences, Guangzhou 510515, China

ABSTRACT

Objective: The probiotic, *Bifidobacterium animalis*, (*B. animalis*) is known to provide health benefits in humans. This study investigated the role of *B. animalis* in suppressing malignant melanoma progression and modulating tumor immunity.

Methods: *Bifidobacterium* spp. were isolated from human faeces and verified by whole-genome sequencing. The anti-tumor effects were assessed in B16-F10 melanoma cells. *B. animalis* efficacy was further evaluated in a syngeneic murine model. Immune profiling was performed with flow cytometry and CD8$^+$ T cell dependency was tested with antibody depletion. Functional metabolites were analyzed by liquid chromatography-mass spectrometry (LC-MS). Transcriptome sequencing elucidated the YAP1 mechanism in CD8$^+$ T cells. Gut microbiota composition was assessed *via* shotgun metagenomic sequencing.

Results: Among the selected *Bifidobacterium* spp., *B. animalis* and its conditioned medium effectively inhibited melanoma cell proliferation. Oral administration of *B. animalis* significantly reduced the growth of B16-F10 allografts, accompanied by an increase in tumor-infiltrating effector T cells. The bioactive component of *B. animalis* was identified as a < 3-kDa non-protein fraction containing mannose, which phenocopied the anti-tumor and immunostimulatory effects of *B. animalis*. Microbiota profiling revealed probiotic enrichment in mannose-treated mice. CD8$^+$ T cell depletion abrogated mannose efficacy. Combination therapy with *B. animalis* and anti-PD-1 synergistically enhanced tumor control and T cell activation. Mechanistically, the bioactive fraction and mannose downregulated YAP1 expression in CD8$^+$ T cells.

Conclusions: *B. animalis* suppresses melanoma tumorigenesis in mice by restoring gut microbiota and secreting functional mannose. Mannose enhances anti-PD-1 efficacy by inhibiting YAP1 expression in CD8$^+$ T cells, thereby improving effector function. *B. animalis* may serve as a preventive measure for melanoma management.

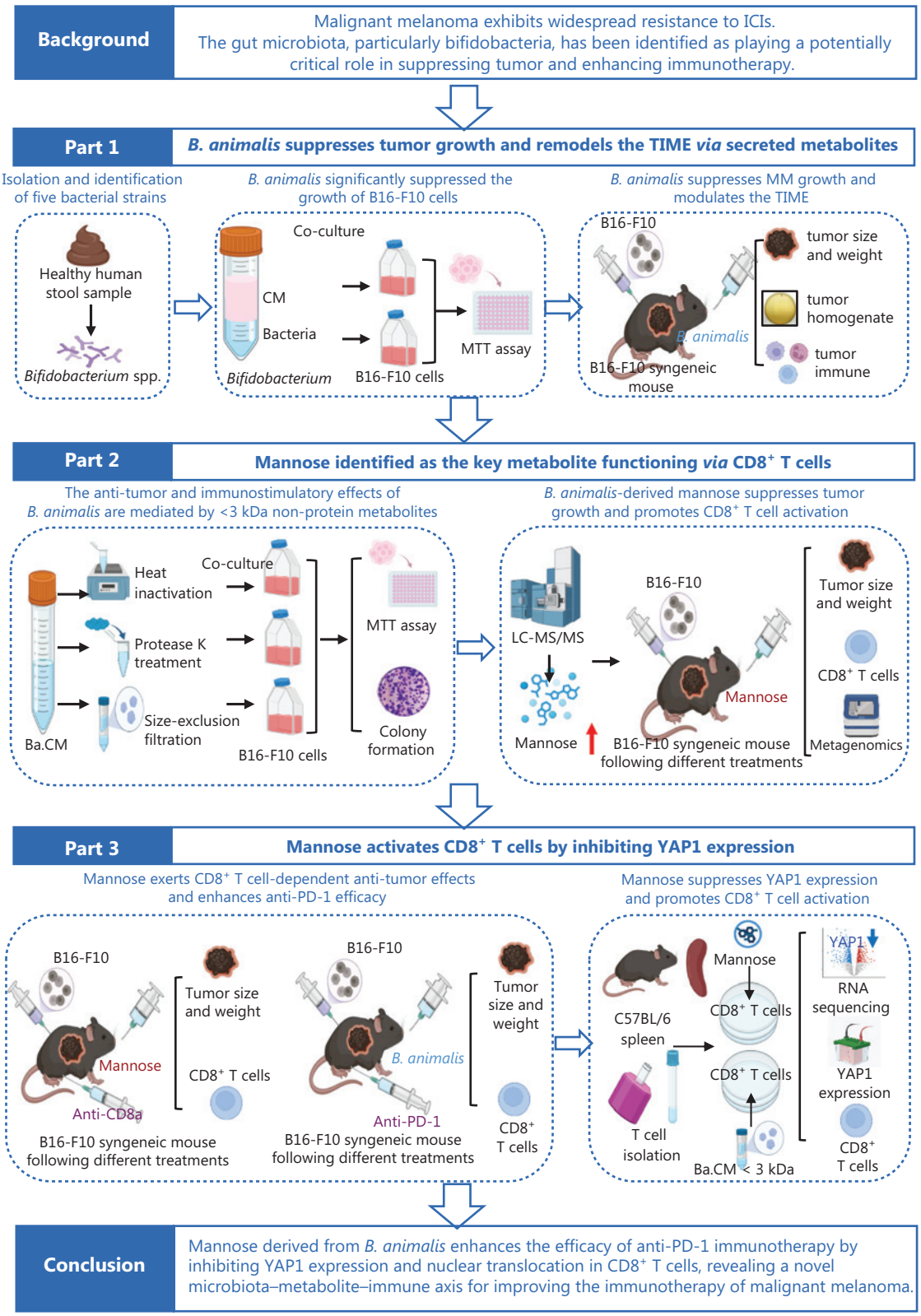
KEYWORDS *Bifidobacterium animalis*; melanoma; mannose; CD8$^+$ T cells; anti-PD-1

Introduction

Malignant melanoma is a highly aggressive and lethal cancer characterized by a high metastatic potential and poor prognosis[1]. Immune checkpoint inhibitors (ICIs), particularly ICIs targeting the programmed death-1 (PD-1)/programmed death-ligand 1 (PD-L1) pathway, have revolutionized systemic treatment of melanoma by reactivating host anti-tumor immunity and reducing immune escape. Despite the remarkable clinical benefits, > 50% of patients develop primary or acquired resistance to ICIs and treatment-related adverse events remain a major clinical challenge[2,3]. The tumor microenvironment (TME), especially the intratumoral immune landscape, has a pivotal role in determining ICI responsiveness[4,5]. Hence, there is an urgent clinical need to identify novel and safe strategies to overcome resistance and enhance ICI efficacy.

Meanwhile, the gut microbiome is increasingly recognized as a critical regulator of systemic immune homeostasis and cancer therapy[6,7]. Accumulating clinical and preclinical evidence

*These authors contributed equally to this work.
Correspondence to: Haijun Deng and Qing Li
E-mail: navyd999@163.com and drliqing@smu.edu.cn
ORCID ID: https://orcid.org/0000-0003-4632-2702 and https://orcid.org/0000-0002-0169-8098
Received October 22, 2025; accepted February 27, 2026;
published online May 6, 2026.
Available at www.cancerbiomed.org
©2026 The Authors. Creative Commons Attribution-NonCommercial 4.0 International License (CC BY-NC 4.0)



Study flowchart *B. animalis*-derived mannose enhances anti-PD-1 efficacy in melanoma by inhibiting YAP1 in CD8+ T cells. **In Part 1**, a human-faeces *B. animalis* isolate is shown to suppress B16-F10 tumors *in vitro* and *in vivo*, concomitantly re-programming the TIME. **Part 2** identifies mannose as the key < 3-kDa immunostimulatory metabolite derived from *B. animalis* that activates CD8+ T cells and enhances

anti-PD-1 efficacy. **Part 3** shows that mannose triggers CD8+ T cell-dependent anti-tumor effects by downregulating YAP1, thereby releasing the Hippo brake on cytotoxicity. Collectively, these findings reveal a novel microbiota–metabolite–immune axis wherein *B. animalis*-derived mannose potentiates anti-PD-1 therapy *via* YAP1 suppression in CD8+ T cells. Abbreviations: *B. animalis*, *Bifidobacterium animalis* , *Ba.CM*, *B. animalis* conditioned medium; CM, conditioned medium; ICIs, immune checkpoint inhibitors; TIME, tumor immune microenvironment. Figure created using BioRender (www.biorender.com).

indicates a close association between gut microbial composition and melanoma progression and responsiveness to ICIs[8,9]. Melanoma patients often exhibit reduced gut microbial diversity that is characterized by a depletion of beneficial commensals, such as *Bifidobacterium*, and an enrichment of potentially pathogenic taxa. Notably, responders to anti-PD-1 therapy consistently show a higher abundance of *Bifidobacterium* and faecal microbiota transplantation (FMT) from responders can restore ICI sensitivity in non-responders, supporting a causal role for gut microbes in promoting anti-tumor immunity[10-12]. Within the genus *Bifidobacterium*, *B. animalis* (Ba) is one of the most widely used and best-characterised probiotic species and is extensively incorporated into fermented dairy products and dietary supplements. In addition to a favorable safety record, Ba has been reported to exert an immunomodulatory effect and help maintain intestinal barrier integrity[13,14]. Preclinical studies further suggest that oral administration of Ba or its metabolite can modulate tumor progression in models of colorectal and lung cancer, accompanied by alterations in the immune microenvironment[15,16].

However, the role of Ba in melanoma, particularly in orchestrating anti-tumor immunity and influencing responses to immune checkpoint blockade, has not been established. To address this gap in knowledge, we aimed to define how Ba, a commensal reduced in melanoma, influences anti-tumor immunity and the response to ICI therapy. In this study the *Ba*-derived metabolite, mannose, was shown to enhance anti-PD-1 efficacy by remodeling the TME to promote $CD8^+$ T-cell infiltration and activation, while also enriching beneficial gut commensals, suggesting a dual mode of action. Mechanistically, mannose was shown to exert immunostimulatory effects by activating the Hippo pathway and functionally inhibiting YAP1 in $CD8^+$ T cells. Collectively, this study provides mechanistic insights into the role of protective bacteria depleted in melanoma patients and offers a novel microbiome-based adjuvant strategy to improve the ICI response.

Materials and methods

Establishment and treatment of the B16-F10 melanoma syngeneic murine model

Six-week-old male C57BL/6 mice (GemPharmatech, Nanjing, Jiangsu, China) were injected subcutaneously with 100 μL of a B16-F10 cell suspension containing 5×10^5 cells into the dorsal flank. Daily oral gavage of Ba or brain heart infusion [BHI] (broth control) began 2 weeks before tumor inoculation and continued until 1 d prior to euthanasia. Tumor volumes were monitored every 2–3 d using digital calipers and calculated as $V = (L \times W^2)/2$, where L is the longest diameter and W is the perpendicular diameter. Faecal samples were collected at regular intervals throughout the study. All mice were sacrificed on day 19, tumors were harvested and weighed, and tissue samples were collected for subsequent immune cell profiling and additional analyses.

Mice received intraperitoneal injections of anti-mouse PD-1 monoclonal antibody (#BE0146; Bio X Cell, Lebanon, NH, USA) or a matched IgG isotype control (#BE0089; Bio X Cell) at a dose of 200 μg per mouse every 3 d when tumor volumes reached 50–100 mm^3.

Anti-mouse CD8α monoclonal antibody (#BE0061; Bio X Cell) was administered intraperitoneally at a dose of 150 μg per mouse twice weekly in the $CD8^+$ T cell depletion model beginning 1 week before tumor cell inoculation.

All animal procedures were approved by the Institutional Animal Care and Use Committee of South China Agricultural University and performed in accordance with relevant guidelines and regulations (Approval No. 2025F818).

Bacterial strains and culture

Ba was obtained from a healthy human stool. The isolation procedure was initiated by homogenizing fresh stool samples in sterile phosphate-buffered saline (PBS). The homogenate was subsequently clarified by filtration through a 100-μm cell strainer. The filtrate was diluted and plated onto *Bifidobacteria* selective media (#90273; Millipore, Burlington, MA, USA) to selectively isolate Ba. *Escherichia coli* strain MG1655 (#700926; ATCC, Manassas, VA, USA), a non-pathogenic commensal bacterium of the human intestine, was used in this study and served as a bacterial control. Ba and the four reference strains were cultured anaerobically in BHI (CM1135B; Oxoid, Basingstoke, Hampshire, UK) at 37°C. Bacterial density was monitored at OD_{600} using a Spectra Max iD3 microplate reader (Molecular Devices, San Jose, CA, USA). Log-phase cultures of Ba were centrifuged at 3,000 g for 10 min and the supernatant was sterile-filtered through 0.22-μm membrane to obtain the conditioned medium (Ba.CM).

Mouse T-cell isolation and activation

Spleens from naïve mice were harvested and processed using a Mouse T Cell isolation kit (#19853; Stemcell Technologies,

Stemcell Technologies, Vancouver, BC, Canada). Purified T cells were then cultured in RPMI-1640 medium supplemented with mouse CD3/CD28 Dynabeads (#11456D; Thermo Fisher Scientific, Waltham, MA, USA) and 30 U/mL of recombinant mouse IL-2 (#575404; BioLegend, San Diego, CA, USA) for activation and expansion.

Tumor-infiltrating immune profiling by flow cytometry

Resected tumor tissues were minced and digested at 37°C for 45 min in a cocktail consisting of 0.5 mg/mL of collagenase D (#C754909; Aladdin, Shanghai, China) and 0.25 mg/mL of DNase I (#10104159001; Roche, Indianapolis, IN, USA) prepared in 1% BSA (Sigma-Aldrich, St. Louis, MO, USA) to generate single-cell suspensions. The digestates were then subjected to filtration and centrifugation at 500 × g for 10 min. Cells were stained with a panel of marker-specific antibodies to delineate myeloid and lymphoid populations, including dendritic cells [DCs] ($CD45^+$ $CD11c^+$ $MHCII^+$), M1 macrophages ($CD45^+$ $CD11b^+$ $F4/80^+$ $CD206^-$), M2 macrophages ($CD45^+$ $CD11b^+$ $F4/80^+$ $CD206^+$), natural killer (NK) cells ($CD45^+$ $CD3^-$ $NK1.1^+$), natural killer T (NKT) cells ($CD45^+$ $CD3^+$ $NK1.1^+$), T regulatory cells [Tregs] ($CD45^+$ $CD3^+$ $CD4^+$ $CD25^+$ $Foxp3^+$), myeloid-derived suppressor cells [MDSCs] ($CD45^+$ $CD11b^+$ $Gr\text{-}1^+$), and $CD8^+$ T cells ($CD45^+$ $CD3^+$ $CD8^+$). The intracellular production of IFN-γ, TNF-α, and granzyme B (GZMB) was measured by flow cytometry to assess immune cell function after stimulation with phorbol 12-myristate 13-acetate [PMA] (50 ng/mL; Sigma-Aldrich, St. Louis, MO, USA), ionomycin (1 μg/mL; Sigma-Aldrich, St. Louis, MO, USA), and monensin (10 μg/mL; Sigma-Aldrich, St. Louis, MO, USA), respectively.

RT2 Profiler qPCR Array

Total RNA was extracted from the tumor tissues using TRIzol™ reagent (15596026; Thermo Fisher Scientific). An RT reagent kit with a gDNA eraser (RR047a; Takara, Kusatsu, Shiga, Japan) was subsequently used to convert the RNA into complementary DNA through reverse transcription. The profiler PCR Arrays for Mouse Inflammatory Response & Autoimmunity (PAMM-077ZC; Qiagen, Hilden, NRW, Germany) were utilized to detect altered gene expression profiles. The experiments were performed on an Applied Biosystem Real-time PCR system (QuantStudio™; Thermo Fisher Scientific).

Cell proliferation and colony formation assay

Cell viability was evaluated using the MTT assay (Thermo Fisher Scientific). B16-F10 cells were plated in 96-well plates at a density of 1×10^3 cells per well and treated with Ba.CM, *E. coli* conditioned medium (Ec.CM), or BHI medium and used as bacteria and broth controls, respectively. Cells were seeded in 6-well plates at a density of 500–1,000 cells per well and exposed to Ba.CM, Ec.CM, or BHI control for 1–2 weeks with medium replenishment every 3 d for the clonogenic survival assay. The number of colonies was quantified using ImageJ software (National Institutes of Health, Bethesda, MD, USA) after fixation and staining with 0.5% crystal violet.

Shotgun metagenomic analysis

Faecal DNA was extracted from mouse stool samples using the Quick-DNA™ Faecal Microbe Miniprep kit (Tiangen Biotech, Beijing, China). Sequencing libraries were constructed and subjected to shotgun metagenomic sequencing on the Illumina MiSeq platform (Illumina, San Diego, CA, USA) in accordance with established protocols[17]. Raw sequencing reads were processed with KneadData (v0.7.2; Harvard T.H. Chan School of Public Health, Boston, MA, USA) to remove host-derived and low-quality sequences, yielding high-quality microbial data. Taxonomic profiling was performed from the quality-filtered reads using MetaPhlAn (v3.0.0; Harvard T.H. Chan School of Public Health, Boston, MA, USA) with the integrated v30 marker database, which enabled accurate characterization of the microbial community composition.

Metabolomic profiling

Untargeted metabolomic analysis was performed using 100 μg of faecal samples (Biotree, Shanghai, China). The extracted metabolites were transferred to a fresh glass vial for liquid chromatography-tandem mass spectrometry (LC MS/MS) analysis. Metabolite separation was achieved using an ultra-high performance liquid chromatography system (Agilent 1290 Infinity Series; Agilent Technologies, Santa Clara, CA, USA) equipped with a UPLC BEH amide column. The mobile phase consisted of 25 mM ammonium acetate and 25 mM ammonium hydroxide in water (pH 9.75) (A) and acetonitrile (B), delivered at a flow rate of 0.5 mL/min. The gradient program was as follows: 0–0.5 min, 95% B; 0.5–7.0 min, from 95%-to-65% B; 7.0–8.0 min, from 65%-to-40% B; 8.0–9.0 min, 40% B; 9.0–9.1 min, from 40%-to-95% B; and 9.1–12.0 min, 95% B. The column temperature was maintained at 25°C, the autosampler at 4°C, and the injection volume was 2 μL. A TripleTOF 6,600 mass spectrometer (AB Sciex, Foster City, CA, USA) was used to acquire MS/MS spectra in an information-dependent acquisition mode. Metabolites were identified by querying an in-house MS2 database, the Human Metabolome Database [HMDB] (www.hmdb.ca), and the METLIN metabolite database (metlin.scripps.edu).

RNA sequencing (RNA-Seq)

Total RNA was extracted with TRIzol (Thermo Fisher Scientific, Waltham, MA, USA) from three biological replicates per group. Libraries were constructed using the TruSeq

Stranded Total RNA kit (Illumina, San Diego, CA, USA) and sequenced on an Illumina HiSeq platform. Differential gene expression was quantified as fragments per kilobase of transcript per million (FPKM) and analyzed using DESeq2 (Bioconductor, Seattle, WA, USA).

Western blotting

Protein lysates from the $CD8^+$ T cells were separated by electrophoresis on 6%–12% gradient SDS-polyacrylamide gels and subsequently transferred to polyvinylidene difluoride (PVDF) membranes (EMD Millipore, Billerica, MA, USA) using a wet transfer system. Membranes were blocked with 5% skim milk prepared in Tris-buffered saline containing 0.1% Tween-20 [TBST] (Solarbio, Beijing, China) for 2 h at room temperature. Immunoblotting was performed using the Hippo Signaling Antibody kit (#HAK21009; Huabio, Hangzhou, Zhejiang, China) with overnight incubation of primary antibodies at 4°C, followed by incubation with corresponding HRP-conjugated secondary antibodies for 1 h at room temperature. Protein bands were visualized using enhanced chemiluminescence (MilliporeSigma, Burlington, MA, USA) substrate and quantified by densitometric analysis.

Statistical analysis

Statistical analyses were performed using GraphPad Prism (version 9.4.1; GraphPad Software, San Diego, CA, USA) and R (version 4.1.1; R Foundation for Statistical Computing, Vienna, Austria). Data are expressed as the mean ± SD with "n" indicating the number of biological replicates. No samples or animals were excluded. An unpaired two-tailed Student's t-test or Mann-Whitney U test was used for comparisons between two groups. Multiple group comparisons were analyzed by ANOVA. A $P < 0.05$ threshold was considered statistically significant. Detailed statistical descriptions are provided in the figure legends.

Results

Healthy human faecal isolated Ba suppresses melanoma progression

Five *Bifidobacterium* species (*Ba*, *B. breve*, *B. bifidum*, *B. longum*, and *B. pseudocatenulatum*) were isolated and identified from healthy human faeces to determine the functional effects of specific bacteria that are depleted in melanoma patients. The bacteria strains were initially confirmed by matrix-assisted laser desorption/ionization-time of flight (MALDI-TOF) MS and subsequently verified by Sanger sequencing (**Figure 1A**). The anti-proliferative effects of these five bacterial were then evaluated. The MTT assay revealed that among the identified bacteria, Ba exhibited the most significant anti-proliferative effect (**Figure 1B**). Furthermore, the Ba.CM demonstrated the strongest inhibitory activity across different concentrations (5% and 10% [vol/vol]; **Figure 1C**), suggesting that Ba has potent anti-melanoma properties.

Ba was administered orally to a B16-F10 syngeneic mouse model in a subsequent experiment. Ba significantly reduced tumor volume and weight compared to the BHI-treated group (**Figure 1D-F**). Tumor tissue was cultured on BHI agar plates to determine whether Ba was present at the tumor site. No viable Ba colonies were detected in the tumor tissues of Ba-treated mice (**Figure 1G**), indicating that the anti-tumor effects of Ba were mediated indirectly through secreted metabolites rather than direct interaction between Ba and tumor cells.

Ba remodels the tumor immune microenvironment (TIME) and directly activates $CD8^+$ T cells via secreted metabolites

A PCR array was performed to profile the expression of 84 key genes involved in the inflammatory response and autoimmunity in syngeneic tumors from Ba- and BHI-treated syngeneic B16-F10 mouse models to elucidate the mechanisms by which Ba suppresses melanoma progression. The analysis revealed that Ba upregulated 22 inflammation-related genes by > 2-fold, while only 1 gene was downregulated (**Figure 2A**). Notably, significant upregulation of immune marker genes associated with CD8+ T cell infiltration (*Cxcl9*, *Cxcl11*, *Ccl19*, and *Ccr7*), NK cell infiltration (*Cxcl11* and *Cxcl19*), Th2 differentiation (IL-19), antigen presentation (IL-1a, IL-1b, *CD40*, and *Fasl*), and Treg regulation (*Ccl22* and *Ccl20*), as well as immunomodulatory factors, including *Tlr7* in allograft tumors from Ba-treated mice (**Figure 2B**) was noted. These findings suggested that Ba may exert tumor-suppressive effects by promoting the enrichment of tumor-infiltrating immune cell populations.

The composition of tumor-infiltrating immune cells was analyzed using multicolor flow cytometry to directly assess the impact of Ba on the tumor immune landscape in melanoma. Ba treatment was confirmed to significantly reduce the populations of MDSCs (**Figure 2C**), tumor-associated macrophages (TAMs), and Tregs (**Figure S1A**). In contrast, the population of $CD8^+$ T cells infiltrating the tumors was significantly enhanced in Ba-treated B16-F10 tumors compared to control treatment (**Figure 2D**). In addition, the frequencies of GZMB-, tumor necrosis factor-alpha (TNF-α)-, and interferon-gamma (IFN-γ)-positive $CD8^+$ T cells were significantly higher in Ba-treated tumors compared to BHI-treated mice (**Figure 2E**), whereas PD-1 expression on tumor-infiltrating $CD8^+$ T cells was not significantly different between the two groups (**Figure S1B**). No significant differences were detected in other immune cell populations, including DCs, M1 macrophages, NK cells, and NKT cells, between BHI- and Ba-treated syngeneic tumors.

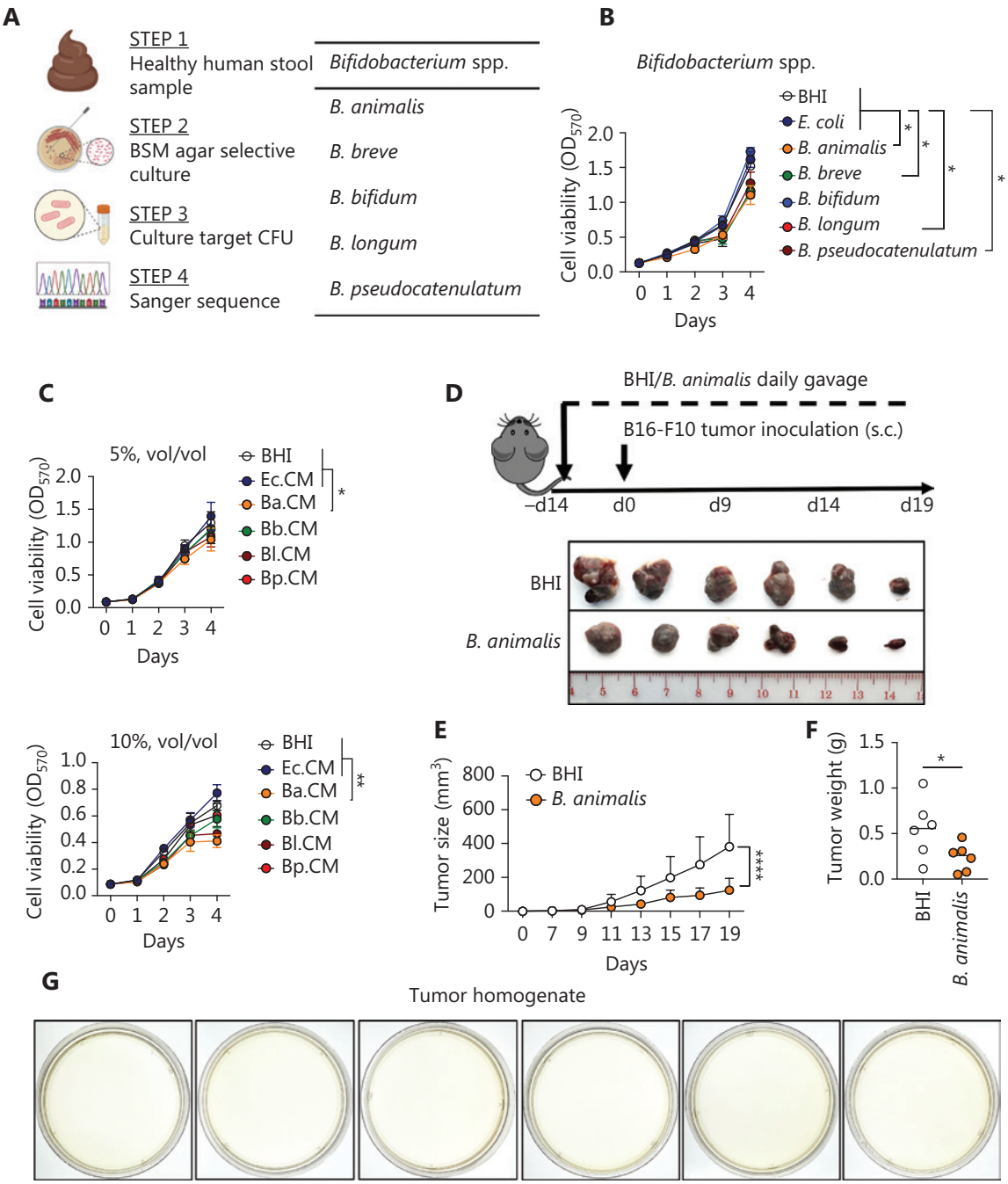


Figure 1 *B. animalis* suppresses melanoma growth and modulates the tumor immune microenvironment *in vitro* and *in vivo*. (A) Identification of bacterial strains isolated from healthy human subjects. (B) MTT assay demonstrates the effect of five *Bifidobacterium* species on B16-F10 cell viability *in vitro* (n = 3). (C) MTT assay demonstrates the influence of CM from five *Bifidobacterium* spp. on B16-F10 cell viability *in vitro* (n = 3). (D) A schematic diagram of the experimental design and timeline for B16-F10 syngeneic mice under various treatments, including representative tumors from each group. (E) Tumor size of B16-F10 syngeneic tumors under various treatments (n = 6). (F) Tumor weight of B16-F10 syngeneic tumors under various treatments (n = 6). (G) Representative images display the bacterial load derived from tumor tissues in the syngeneic tumor model. The LOD was determined to be 10 CFU/mL based on the plating of 100 μL of undiluted tissue homogenate. *, $P < 0.05$; **, $P < 0.01$. The data are presented as the mean ± SD. Statistical significance was assessed using an unpaired t-test, one-way analysis of variance, or two-way analysis of variance, as indicated. Abbreviations: *B. animalis*, *Bifidobacterium animalis*; BHI, brain heart infusion; CFU, colony-forming units; CM, conditioned medium; LOD, limit of detection; SD, standard deviation.

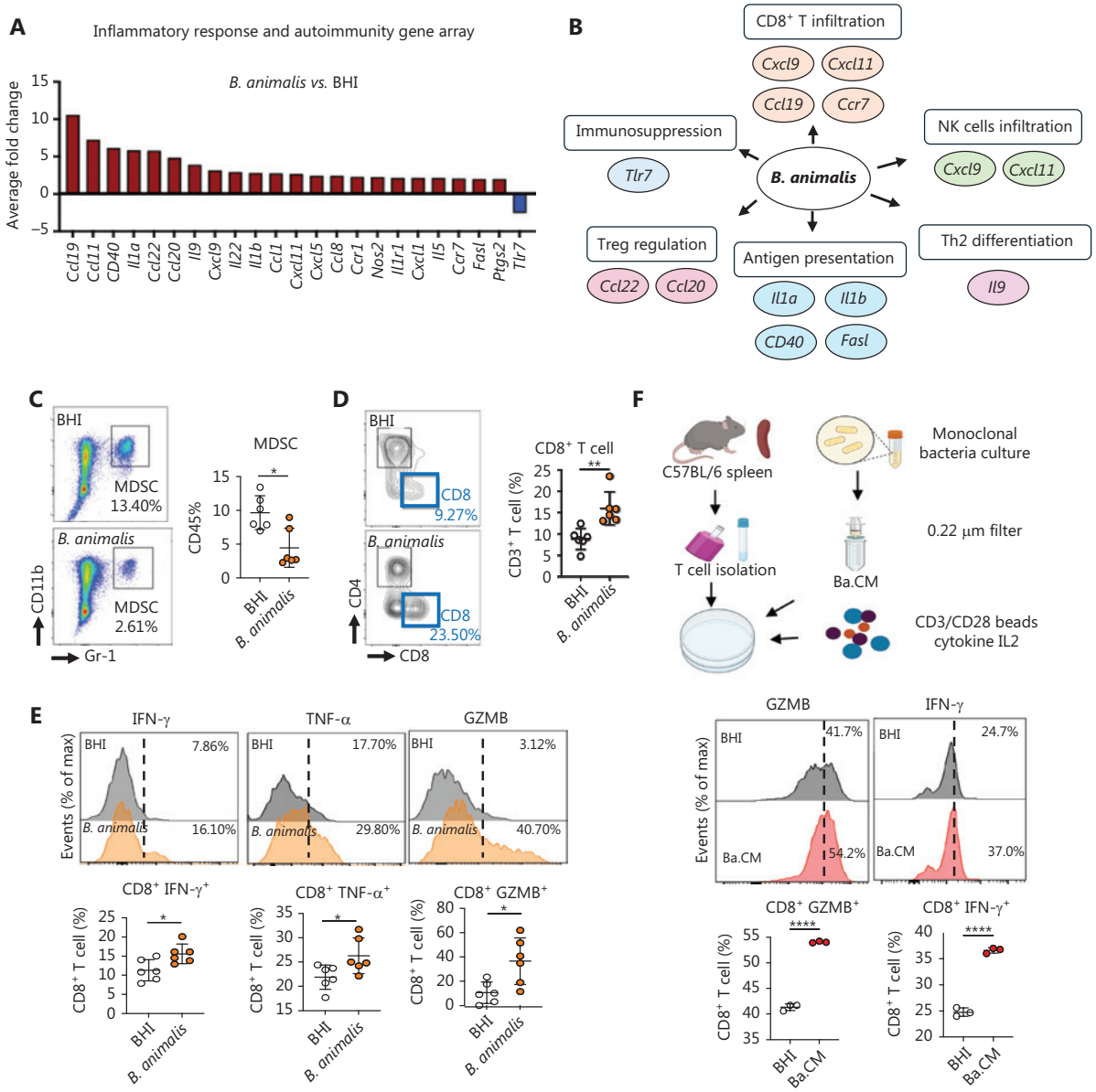


Figure 2 *B. animalis* modulates the tumor immune microenvironment in B16-F10 melanoma by promoting CD8⁺ T cell activation. (A) Differential expression of inflammatory response and autoimmunity-related genes between the *B. animalis* and BHI control groups, as profiled by the inflammatory response and autoimmunity gene PCR array. (B) Network diagram of *B. animalis*-modulated immune signaling. The network highlights key alterations in the TIME compared to the BHI control, emphasizing enhanced CD8⁺ T and NK cell infiltration, promotion of Th2 differentiation, and modulation of Treg activity and antigen presentation. These processes are mediated by upregulated chemokines (*Cxcl9*, *Cxcl11*, *Cxcl19*, *Cxcl22*, and *Ccl20*) and immunosuppressive factors (*Tlr7*). (C) Flow cytometric analysis revealed a significant reduction in MDSCs within B16-F10 tumors from *B. animalis*-treated mice compared to the BHI control group (n = 6). (D) Flow cytometric analysis revealed a significant increase in CD8⁺ T cell infiltration within B16-F10 tumor tissues from *B. animalis*-treated mice compared to the BHI control group (n = 6). (E) Flow cytometry analysis demonstrated a significant increase in the frequency of GZMB, TNF-α, and IFN-γ-expressing CD8⁺ T cells within tumor tissues of *B. animalis*-treated B16-F10 mice compared to the BHI control group (n = 6). (F) Schematic illustration of CD8⁺ T cell isolation from mouse spleen and subsequent activation assay. Flow cytometric analysis confirms the direct *in vitro* activation of CD8⁺ T cells by Ba.CM compared to the BHI control (n = 3). *, $P < 0.05$; **, $P < 0.01$; ****, $P < 0.0001$. Data are presented as the mean ± SD. Statistical significance was assessed using an unpaired t-test, one-way analysis of variance, or two-way analysis of variance, as indicated. *B. animalis*, Bifidobacterium animalis; BHI, brain heart infusion; *Ba.CM*, *B. animalis* conditioned medium; GZMB, granzyme B; IFN-γ, interferon-gamma; MDSCs, myeloid-derived suppressor cells; NK, natural killer; SD, standard deviation; TNF-α, tumor necrosis factor-alpha; TIME, tumor immune microenvironment.

The direct immunomodulatory effects of Ba was further investigated on melanoma, given the central role of effector T cells in tumor immunotherapy. $CD8^+$ T cells were isolated from mouse spleens and stimulated *in vitro* with Ba.CM. Direct activation of $CD8^+$ T cells was noted upon treatment with Ba.CM, which was characterized by significantly enhanced expression of the effector molecules GZMB and IFN-γ in purified $CD8^+$ T cells (**Figure 2F**). Taken together, these results underscored the potential of Ba as a therapeutic agent for enhancing anti-tumor immunity in melanoma.

The anti-tumor and immunostimulatory effects of Ba are mediated by < 3 kDa non-protein metabolites

Ba.CM was first stripped of protein function by subjecting the Ba.CM to proteolytic digestion (proteinase K, 50 μg/mL; Sigma-Aldrich, St. Louis, MO, USA) or heat inactivation (100°C for 30 min) to identify the bioactive metabolite(s) associated with the observed anti-cancer and immune-boosting activity. Neither treatment diminished the suppression of B16-F10 proliferation or clonogenic survival (**Figure 3A, B**), confirming that the effector molecule(s) are non-proteinaceous. Subsequent size-fractionation through 50-, 30- and 3-kDa cut-off membranes showed that only the < 3 kDa permeate reproduced the full cytostatic activity, whereas the > 50 kDa retentate and the 3–50 kDa fraction were inactive (**Figure 3C, D**). The same low-molecular-weight, non-protein pool also elicited direct $CD8^+$ T-cell activation, doubling the frequencies of TNF-α^+ and IFN-γ^+ cells (**Figure 3E**). Thus, tumor suppression and immune stimulation by Ba are mediated by < 3 kDa non-protein metabolites.

Mannose is the Ba-secreted metabolite that restrains melanoma and promotes intratumoral $CD8^+$ T cell activation

Untargeted metabolomics was performed on Ba.CM and stool samples collected from melanoma tumor-bearing mice under different treatments to pinpoint the functional metabolites that translate the anti-melanoma and immunomodulatory activity of Ba into action. Among the differentially accumulated features, mannose emerged as the most prominently enriched metabolite in both matrices (**Figure 4A, B**). Targeted quantification corroborated these findings, which showed a robust elevation of mannose in Ba.CM (**Figure 4C, left**) and faecal samples from Ba-treated mice (**Figure 4C, right**).

We next asked whether mannose is sufficient to reproduce the probiotic phenotype. Importantly, supplementary experiments showed that administration of 1% mannose in drinking water increased mannose levels in serum (**Figure S2A**) and the TME (**Figure S2B**) to levels comparable to the levels induced by oral gavage of Ba. Consequently, this 1% mannose regimen was adopted for all subsequent *in vivo* studies. Mice challenged subcutaneously with B16-F10 cells received mannose in the drinking water (**Figure 4D**). Mannose-exposed tumor-bearing mice exhibited a marked reduction in tumor volume (**Figure 4E**) and tumor weight (**Figure 4F**) compared to the control group. Multicolor flow cytometry of dissociated tumors revealed that mannose not only increased the frequency of intratumoral $CD8^+$ T cells (**Figure 4G**) but also raised the fraction of $CD8^+$ T cells producing GZMB, TNF-α, and IFN-γ (**Figure 4H**), indicating simultaneous enhancement of T-cell infiltration and activation. Taken together, these data established mannose as a key bioactive metabolite released by Ba that directly curtails melanoma growth by re-programming the TIME toward productive $CD8^+$ T-cell immunity.

Mannose reshapes the gut microbiota of B16-F10 tumor-bearing mice

Faecal samples were profiled by shotgun metagenomic sequencing to determine whether the anti-tumor effects of Ba-derived mannose is relayed through the gut microbiota. α-diversity metrics (observed species, Ace, Chao1, Shannon, Simpson, and Goods coverage) were indistinguishable between vehicle- and mannose-treated mice (**Figure 5A**). In agreement with this finding, principal coordinates analysis (PCoA) based on Bray–Curtis dissimilarity indicated substantial overlap in overall microbial community structure between the two groups (PC1: 47.22%; PerMANOVA $P = 0.22$; **Figure 5B**), suggesting that mannose does not perturb the overall architecture of the microbiota. Taxonomic profiling further revealed that mannose treatment led to a significant increase in the abundance of beneficial bacteria belonging to the *Lactobacillus* genus (**Figure 5C**). Differential-abundance testing (DESeq2; false discovery rate [FDR] < 0.05) pinpointed three immunostimulatory taxa as the main drivers (Ba, *B. pseudocatenulatum*, and *L. rhamnosus*; **Figure 5D**). A mouse-wise heat-map ($\log_2$-transformed relative abundance) confirmed that mannose selectively and consistently enriched these probiotic species. Taken together, these findings demonstrated that mannose does not induce broad changes in gut microbial ecology even though mannose drives the selective enrichment of beneficial bacteria with recognized immunomodulatory properties. This prebiotic-like activity provides a plausible mechanistic link between mannose-induced microbiota shifts and the previously observed anti-tumor and immune-activating effects.

Mannose exerts anti-tumor effects through $CD8^+$ T cell-dependent mechanisms and Ba enhances anti-PD-1 efficacy in a B16-F10 syngeneic mouse model

A $CD8^+$ T cell-depleted B16-F10 syngeneic model was established to determine whether $CD8^+$ T cells mediate the

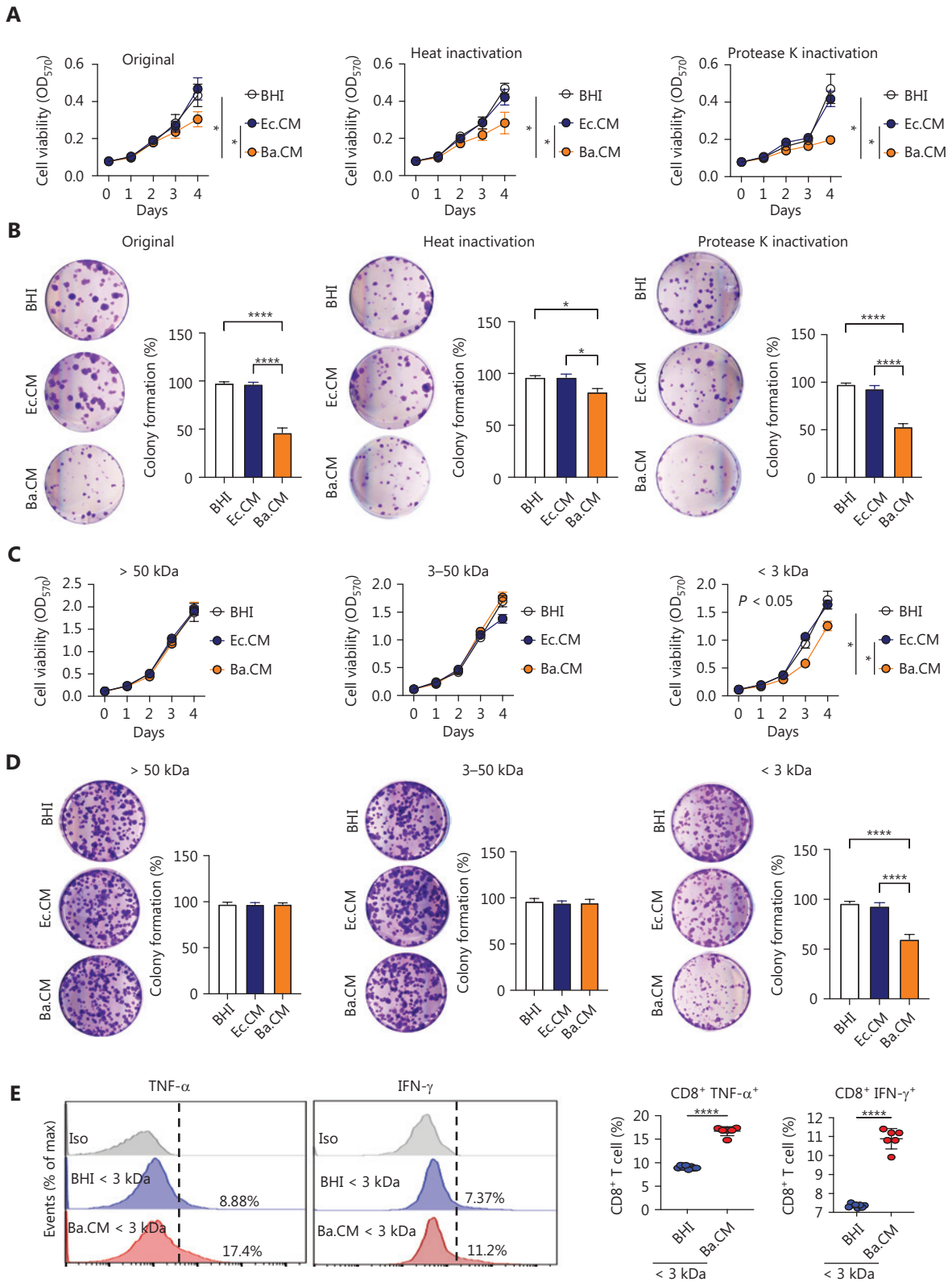


Figure 3 *B. animalis* secretes < 3 kDa non-protein metabolites that suppress melanoma growth and activate CD8⁺ T cells. (A, B) Ba.CM retained inhibitory activity against B16-F10 cell viability (A) and colony formation (B) after protease K (PK) digestion or heat inactivation (n = 3). (C, D) The < 3 kDa fraction of Ba.CM (Ba.CM < 3 kDa) effectively suppressed B16-F10 cell viability (C) and colony formation (D) (n = 3).

(E) Ba.CM < 3 kDa directly activated CD8$^+$ T cells and increased the proportion of TNF-α^+ and IFN-γ^+ cells (n = 6). *, P < 0.05; ****, P < 0.0001. Data are presented as the mean ± SD. Statistical significance was assessed using an unpaired t-test, one-way analysis of variance, or two-way analysis of variance, as indicated. Abbreviations: *B. animalis*, *Bifidobacterium animalis*; BHI, brain heart infusion; *Ba.CM*, *B. animalis* conditioned medium; *Ec.CM*, *E. coli* conditioned medium; GZMB, granzyme B; IFN-γ, interferon-gamma; SD, standard deviation; TNF-α, tumor necrosis factor-alpha.

anti-tumor activity of mannose. Tumor-bearing mice received twice-weekly intraperitoneal injections of anti-CD8α monoclonal antibody combined with daily oral gavage of vehicle or mannose (**Figure 6A**). Mannose treatment mildly suppressed tumor growth under CD8$^+$ T cell-depleted conditions with limited effects on tumor size and weight compared to the control groups (**Figure 6B-D**). Flow cytometric analysis confirmed efficient depletion of CD8$^+$ T cells in peripheral blood and tumor tissues (**Figure 6E, F**). These results demonstrated that the anti-tumor efficacy of mannose is primarily dependent on CD8$^+$ T cells.

Building on the finding that Ba-derived mannose promotes CD8$^+$ T-cell fitness, whether this probiotic could serve as a biological adjuvant to sensitize tumors to anti-PD-1 treatment was determined (**Figure 6G**). A combination therapy model was established in which tumor-bearing mice received daily oral gavage of BHI or Ba. Mice were treated with twice-weekly intraperitoneal injections of anti-mouse PD-1 monoclonal antibody when tumor volumes reached 50–100 mm^3. The combination of Ba with anti-PD-1 resulted in significantly greater tumor suppression in B16-F10 tumor-bearing mice compared to monotherapy or control treatments (**Figure 6H-J**). This enhanced anti-tumor effect was associated with substantially increased infiltration and activation of effector CD8$^+$ T cells within tumors (**Figure 6K**). These findings indicated that Ba sensitizes melanoma to anti-PD-1 therapy by remodeling the TIME and enhancing CD8$^+$ T cell-mediated cytotoxicity.

Ba and its derived mannose inhibit YAP1 to promote CD8$^+$ T cell activation

Dose–response experiments were performed and 1 mM was identified as the concentration producing the most robust enhancement of CD8$^+$ T cell function to dissect how mannose reprogrammed CD8$^+$ T cell anti-tumor immunity (**Figure S3A**). Splenic CD8$^+$ T cells were isolated from C57BL/6 mice, treated with mannose (1 mM) for 24 h, and bulk RNA sequencing was performed. Differential gene expression was revealed by transcriptomic analysis across treatment conditions (**Figure 7A**) with volcano plot analysis confirming widespread transcriptional alterations (**Figure 7B**) and quantitative analysis demonstrating a reduction in YAP1 mRNA levels (**Figure 7C**). YAP1 is a documented negative regulator of effector function[18]. This finding was validated with the Ba.CM < 3 kDa fraction or purified mannose (1 mM); both reagents led to a significant reduction in YAP1 expression (**Figure 7E, G**). Gene set enrichment analysis (GSEA) revealed significant enrichment of the Hippo signaling gene set in mannose-treated CD8$^+$ T cells (**Figure 7D**). Because YAP1 is a key downstream effector of the Hippo signaling pathway, decreased expression of YAP1 was accompanied by prominent phosphorylation at Ser127, a critical site associated with functional inactivation and cytoplasmic retention[19]. Concomitantly, a decline in total YAP1/TAZ protein levels was demonstrated in CD8$^+$ T cells. The nuclear trans-localization of YAP was also significantly diminished in CD8$^+$ T cells upon treatment with mannose or Ba.CM (**Figure 7E, G**). The upstream kinases were also examined by western blotting to further substantiate activation of the canonical Hippo kinase cascade and increased phosphorylation of Lats1 was observed in CD8$^+$ T cells following mannose or the Ba.CM < 3 kDa fraction treatment (**Figure 7E, G**). Functional assessment through *in vitro* co-culture assays demonstrated that Ba.CM < 3 kDa and mannose significantly enhanced CD8$^+$ T cell effector function with substantial increases in the percentages of IFN-γ^+, TNF-α^+, and GZMB$^+$ cells (**Figure 7F, H**). These findings collectively suggested that the Ba.CM < 3 kDa fraction and mannose enhance CD8$^+$ T cell activation *via* the Hippo signaling pathway, mediated through downregulation of YAP1 and subsequent sequestration in the cytoplasm, thereby preventing nuclear translocation and transcriptional activity (**Figure 8**). It has been reported that mannose uptake is predominantly mediated by glucose transporters (GLUTs), particularly GLUT1[20]. Pharmacologic inhibition experiments were performed using the GLUT1-specific inhibitor, BAY-876, to validate the necessity of GLUT1-mediated uptake for the biological effects of mannose. GLUT1 blockade largely abrogated the functional enhancement of CD8$^+$ T cells induced by mannose or the Ba.CM < 3 kDa fraction. Specifically, upregulation of key effector molecules (IFN-γ, TNF-α, and GZMB) was significantly reduced in the presence of BAY-876 (**Figure S4A, B**). Concomitantly, BAY-876 eliminated mannose- and Ba.CM < 3 kDa fraction-induced modulation of the Hippo-YAP1 axis, marked by attenuated Lats1 phosphorylation and impaired YAP1 Ser127 phosphorylation, downregulation, and nuclear exclusion (**Figure S4C**). These results clearly confirmed that GLUT1-mediated mannose uptake is a prerequisite for engaging the Hippo-YAP1 axis and boosting CD8$^+$ T cell effector function (**Figure 8**).

Discussion

Despite the established role of immune checkpoint blockade targeting PD-1/PD-L1 in melanoma therapy, a substantial

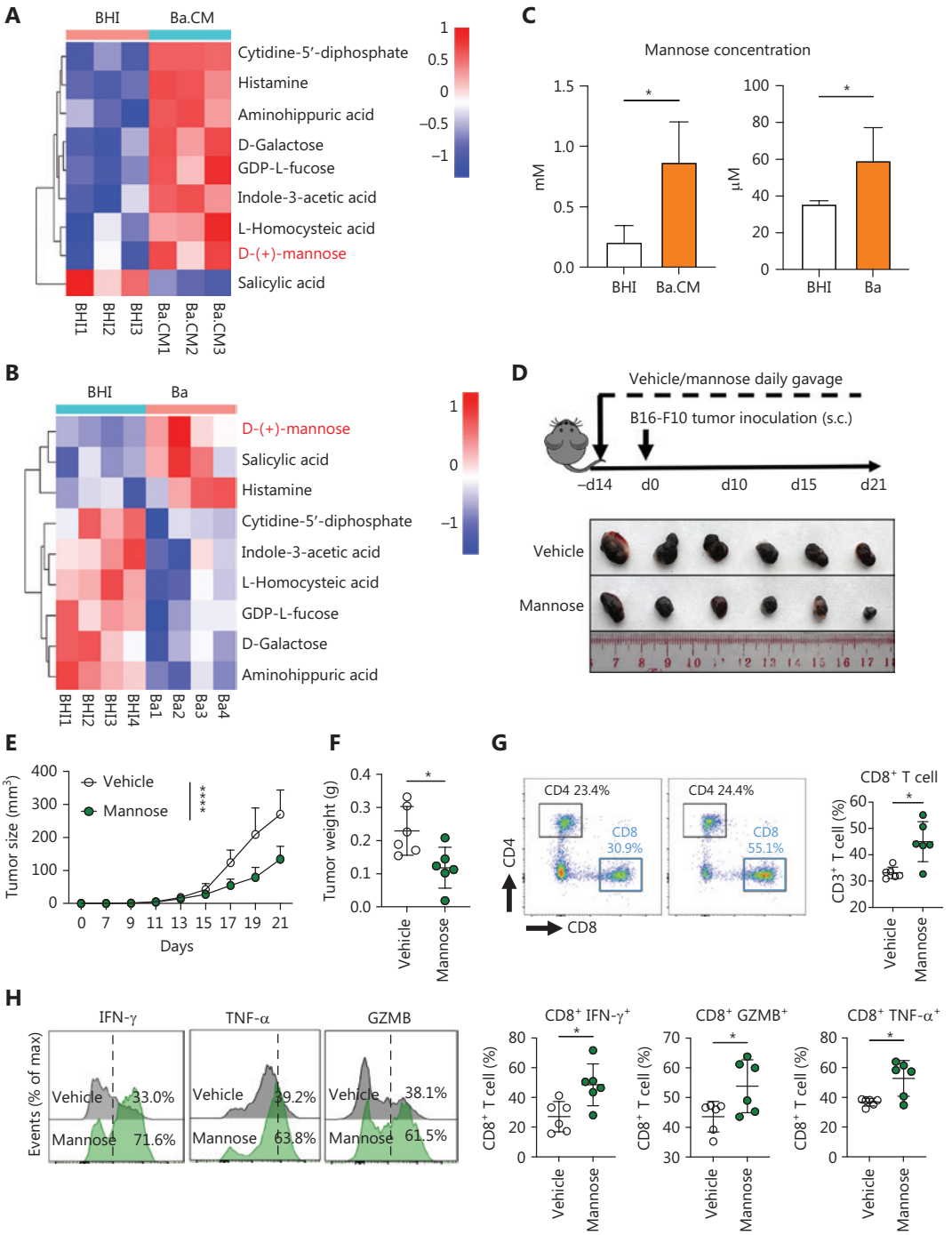


Figure 4 *B. animalis*-derived mannose suppresses tumor growth and promotes CD8⁺ T cell activation. (A) Untargeted metabolomic analysis revealed significant enrichment of mannose in Ba.CM (n = 3). (B) Elevated mannose levels were detected in faecal samples from *B. animalis*-treated mice (n = 4). (C) Targeted metabolomic quantification of mannose in bacterial conditioned medium and faecal samples (n = 3). (D) Schematic diagram depicting the experimental design and timeline for mannose treatment in the B16-F10 syngeneic mouse model, including representative tumors from each group. (E, F) Oral administration of mannose significantly inhibited tumor growth in the B16-F10 model, as shown by reduced Tumor volume (E) and Tumor weight (F) (n = 6). (G, H) Flow cytometry analysis demonstrated that mannose treatment enhanced both infiltration (G) and activation (H) of CD8⁺ T cells within TIME (n = 6). *, P < 0.05; ****, P < 0.0001. Data are presented as the mean ± SD. Statistical significance was assessed using an unpaired t-test, one-way analysis of variance, or two-way analysis of variance, as indicated. Abbreviations: *B. animalis*, *Bifidobacterium animalis*; BHI, brain heart infusion; *Ba.CM*, *B. animalis* conditioned medium; GZMB, granzyme B; IFN-γ, interferon-gamma; SD, standard deviation; TNF-α, tumor necrosis factor-alpha.

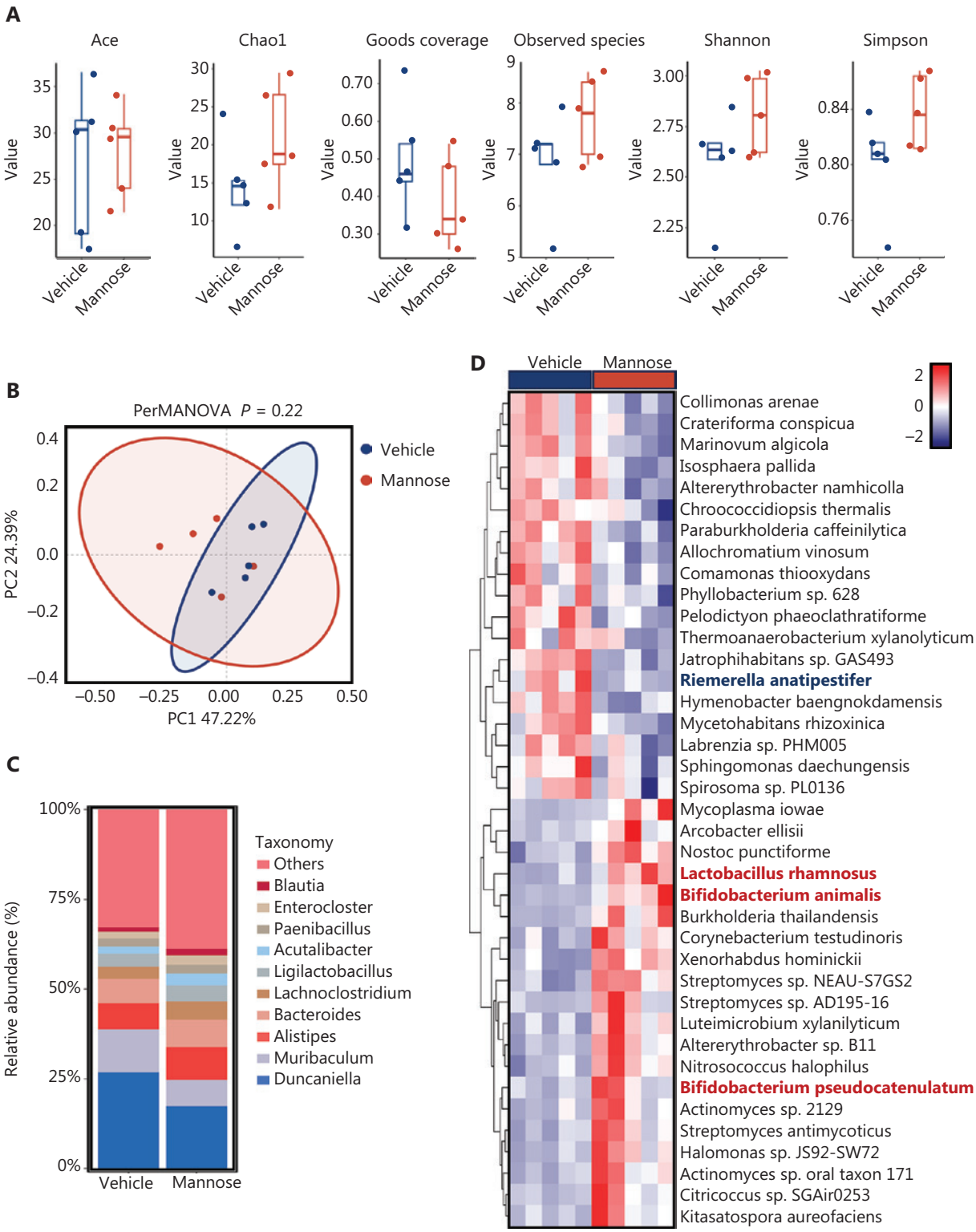


Figure 5 *B. animalis*-derived mannose modulates gut microbiota composition. (A) Analysis of α-diversity indices (observed species, Ace, Chao1, Shannon, Simpson, and Goods coverage) in faecal samples from vehicle- and mannose-treated mice (n = 5). (B) Principal coordinates analysis (PCoA) based on Bray–Curtis dissimilarity showing microbial community separation between groups (PC1: 47.22%; PerMANOVA P = 0.22) [n = 5]. (C) Comparative profiling of predominant bacterial genera at the genus level between the vehicle and mannose groups. (D) Heatmap depicting species-level bacterial composition. Rows represent bacterial species, columns correspond to individual mouse samples, and color intensity indicates $\log_2$-transformed relative abundance (n = 5).

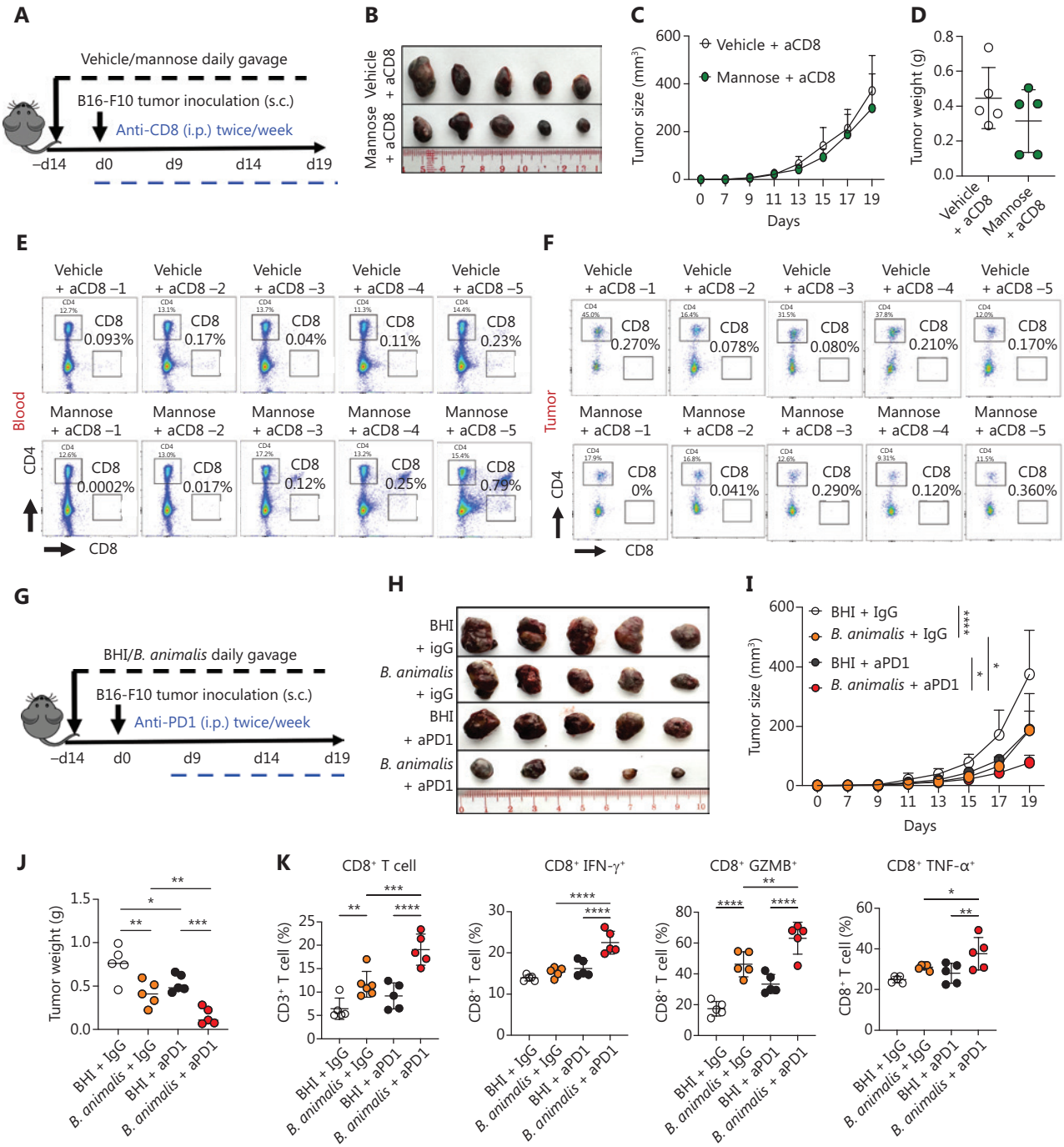


Figure 6 Mannose exerts CD8⁺ T cell-dependent anti-tumor effects and *B. animalis* enhances anti-PD-1 efficacy. (A) Schematic diagram depicting the experimental design and timeline for CD8⁺ T cell depletion in the B16-F10 syngeneic mouse model. (B) Representative Tumor images from each treatment group (n = 5). (C, D) Tumor volume (C) and weight (D) in CD8⁺ T cell-depleted mice following mannose treatment (n = 5). (E, F) Flow cytometric confirmation of successful CD8⁺ T cell depletion in peripheral blood (E) and tumor tissues (F) (n = 5). (G) Schematic diagram illustrating the combined therapeutic regimen of *B. animalis* and anti-PD-1. (H) Representative tumors from combined treatment groups (n = 5). (I, J) Tumor size (I) and weight (J) following combination therapy with *B. animalis* and anti-PD-1 (n = 5). (K) Combination therapy with *B. animalis* and anti-PD-1 significantly enhanced tumor infiltration and activation of effector CD8⁺ T cells (n = 5). *, $P < 0.05$; **, $P < 0.01$; ***, $P < 0.001$; ****, $P < 0.0001$. Data are presented as the mean ± SD. Statistical significance was assessed using an unpaired t-test, one-way analysis of variance, or two-way analysis of variance, as indicated. Abbreviations: *B. animalis*, *Bifidobacterium animalis*; BHI, brain heart infusion; GZMB, granzyme B; IFN-γ, interferon-gamma; SD, standard deviation; TNF-α, tumor necrosis factor-alpha.

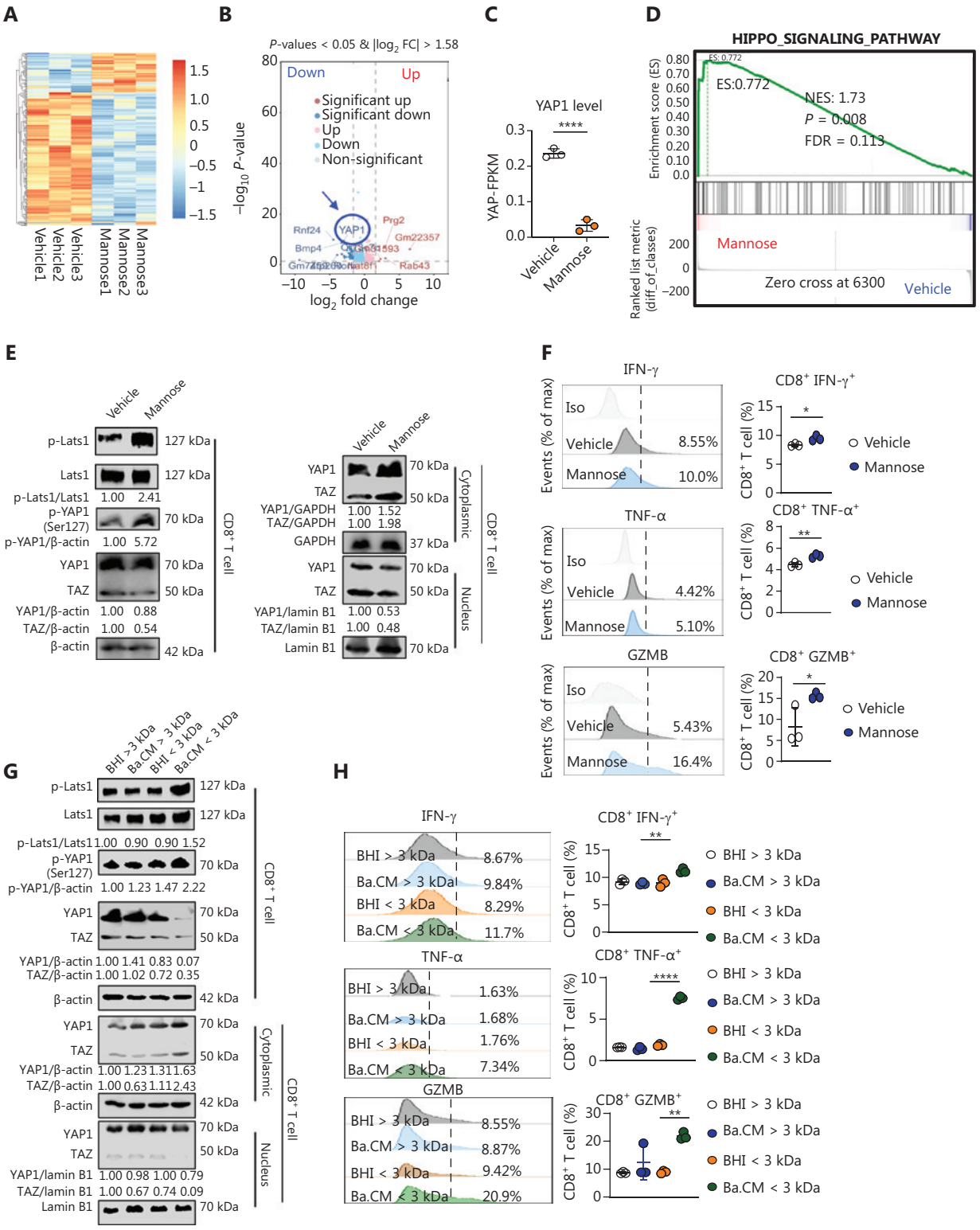


Figure 7 *B. animalis* and its derived mannose suppress YAP1 expression and promotes CD8⁺ T cell activation. (A) Heatmap of differentially expressed genes from transcriptome sequencing analysis (n = 3). (B) Volcano plot displaying genome-wide transcriptional alterations. (C) YAP1 expression levels following mannose treatment (n = 3). (D) GSEA plot showing significant enrichment of the Hippo signaling pathway in mannose-treated CD8⁺ T cells compared to the vehicle group (NES = 1.73, P = 0.008). (E) Mannose induces phosphorylation of YAP at

Ser127 and inhibited nuclear translocation. Mannose reduces YAP1/TAZ protein levels and nuclear localization. (F) *In vitro* co-culture assays demonstrate that mannose significantly upregulates IFN-γ, TNF-α, and GZMB expression in $CD8^+$ T cells (n = 3). (G) Ba.CM < 3 kDa fraction induces YAP phosphorylation at Ser127 and suppresses nuclear translocation, reducing both YAP1/TAZ protein expression and nuclear accumulation. (H) *In vitro* co-culture assays confirm that Ba.CM < 3 kDa markedly enhances IFN-γ, TNF-α, and GZMB expression in $CD8^+$ T cells (n = 3). *, $P < 0.05$; **, $P < 0.01$; ****, $P < 0.0001$. Data are presented as the mean ± SD. Statistical significance was assessed using an unpaired t-test, one-way analysis of variance, or two-way analysis of variance, as indicated. FPKM, fragments per kilobase of transcript sequence per million mapped fragments. Abbreviations: *B. animalis*, *Bifidobacterium animalis*; BHI, brain heart infusion; *Ba.CM*, *B. animalis* conditioned medium; GSEA, Gene set enrichment analysis; GZMB, granzyme B; IFN-γ, interferon-gamma; SD, standard deviation; TNF-α, tumor necrosis factor-alpha.

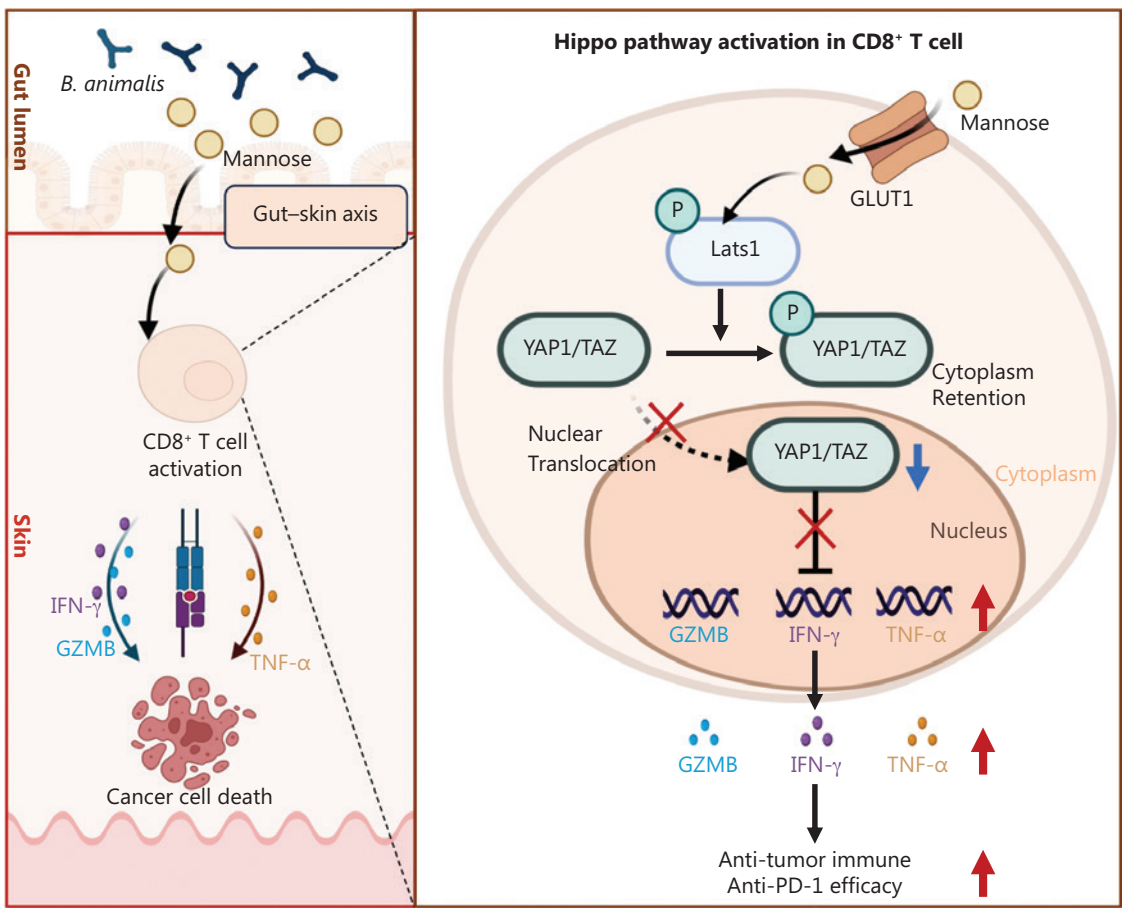


Figure 8 Schematic illustration of the mechanism by which *B. animalis*-derived mannose enhances anti-tumor immunity and anti-PD-1 efficacy. *B. animalis* releases mannose in the gut lumen, which is transported to the skin tumor microenvironment *via* the gut–skin axis. This systemic crosstalk leads to $CD8^+$ T cell activation and subsequent cancer cell death. The right panel details Hippo pathway activation in $CD8^+$ T cells. Extracellular mannose enters the cytoplasm through the GLUT1 transporter. Intracellular mannose promotes the phosphorylation (P) of Lats1, which subsequently phosphorylates YAP1/TAZ. Phosphorylated YAP1/TAZ is retained in the cytoplasm, restricting nuclear localization and consequently relieving nuclear YAP1-mediated repression of effector gene transcription, including GZMB, IFN-γ, and TNF-α. Restoration of these effector programs potentiates $CD8^+$ T cell cytotoxicity. Collectively, this signaling cascade promotes $CD8^+$ T cell activation, leading to a significant increase in overall anti-tumor immune responses and anti-PD-1 efficacy. Abbreviations: *B. animalis*, *Bifidobacterium animalis*; GZMB, granzyme B; GLUT1, glucose transporter 1; IFN-γ, interferon-gamma; Lats1, large tumor suppressor kinase 1; PD-1, programmed cell death-1; TAZ, transcriptional coactivator with PDZ-binding motif; TNF-α, tumor necrosis factor-alpha; YAP1, Yes-associated protein 1. Figure created using BioRender (www.biorender.com).

proportion of patients exhibit limited clinical responses. Recent advances have highlighted the gut microbiome as a key modulator of immunotherapy efficacy, with FMT demonstrating potential in overcoming anti-PD-1 resistance[11]. Among commensal microbes, *Bifidobacterium* spp. has been implicated in enhancing antitumor immunity and synergizing with anti-PD-L1 therapy[10]. However, the precise species conferring these benefits have remained unclear. Notably, the current study identified Ba as a potent immunomodulatory probiotic that significantly augments anti-PD-1 efficacy and suppresses melanoma progression in preclinical models.

It is widely recognized that microbiota-derived metabolites serve as chemical messengers bridging the microscopic microbial community and macroscopic host health[21]. Moving beyond genus-level associations, we mechanistically dissected the metabolite-mediated communication between Ba and host immunity. Remarkably, a low-molecular-weight (< 3 kDa) metabolite fraction responsible for the observed anti-tumor and T cell-stimulating effects was identified. Untargeted metabolomics revealed significant enrichment of mannose in Ba.CM and faecal samples from Ba-treated mice compared to the controls. The findings demonstrated that mannose enters $CD8^+$ T cells *via* GLUT transporters (primarily GLUT1), where mannose functions as a signaling modulator to regulate the Hippo-YAP1 axis, thereby enhancing T-cell effector functions. Recent studies have also reported that mannose can inhibit glycolysis and redirect carbon flux toward the TCA cycle independent of fatty acid oxidation at the metabolic level, thereby improving mitochondrial fitness in T cells, suggesting that mannose can function as a metabolic and a direct signaling molecule within cells[22]. While previous studies have reported the direct anti-tumor activity of mannose[23,24], mannose supplementation was noted to enrich beneficial commensals, such as *Bifidobacterium*, supporting a dual mechanism of action (direct $CD8^+$ T cell activation and indirect remodeling of the gut microbiome). It has become clear that *Bifidobacterium* can serve as adjuvants in cancer prevention by modulating the gut microbiota and enhancing the host immune response[25], suggesting that mannose may sustain a favorable microbial ecosystem that further amplifies anti-tumor immunity. Nevertheless, whether the observed microbial shifts reflect a direct prebiotic effect of mannose or arise secondarily from immune reprogramming and reduced tumor burden remains to be determined.

A pivotal finding was that $CD8^+$ T cell depletion almost completely abrogated the mannose anti-tumor effects, underscoring a T cell-dependent mechanism. Notably, a modest, non-significant residual inhibitory trend on subcutaneous tumor growth persisted after $CD8^+$ T cell depletion ($P > 0.05$), which may reflect $CD8^+$ T cell-independent contributions, such as a direct anti-proliferative effect of mannose on tumor cells, partial modulation of other immune compartments, and mannose-associated remodeling of the gut microbiota. The findings demonstrated that oral administration of Ba significantly enhances the infiltration and activation of $CD8^+$ T cells within the TME in a murine melanoma model. An anti-PD-1 treatment model was established given the known correlation between $CD8^+$ T cell activation and response to PD-1 blockade[26]. Remarkably, the combination of Ba and anti-PD-1 therapy resulted in more effective tumor suppression. This synergistic effect demonstrated that modulation of the gut microbiota can enhance the efficacy of immune checkpoint blockade, likely through potentiation of $CD8^+$ T cell function. Furthermore, the current study provided mechanistic evidence that Ba remodels the TIME, potentially overcoming resistance to monotherapy. The novelty of this work lies in proposing a translatable microbiota-targeted strategy that augments current immunotherapeutic regimens without significant additional toxicity. These results not only establish Ba as a promising adjuvant in melanoma immunotherapy but also highlight the broad potential of microbiome-based interventions to improve treatment outcomes by enhancing T cell-mediated anti-tumor immunity.

Strikingly, mannose emerged as a previously unrecognized microbial metabolite that suppresses the Hippo pathway in $CD8^+$ T cells. Specifically, mannose reduces YAP1 transcription and promotes YAP1 (Ser127) phosphorylation, thereby preventing nuclear accumulation. The mannose-induced cytosolic retention explains the increased frequency of IFN-γ-, TNF-α-, and GZMB-producing effector T cells observed following treatment given that nuclear YAP1 restricts $CD8^+$ T cell cytotoxicity[18,27]. These findings reinforce the link between microbial products and Hippo signaling and further identify mannose as a diet-accessible, probiotic-derived metabolite that releases an intrinsic brake on anti-tumor immunity. Previous pharmacokinetic studies suggested that oral mannose administration is efficiently absorbed into the circulation and cleared mainly *via* hepatic metabolism and renal excretion. Given the increased vascular permeability and altered nutrient accessibility of the TME, Circulating mannose is likely available to tumor-infiltrating immune cells at biologically relevant concentrations given that nuclear YAP1 restricts $CD8^+$ T cell cytotoxicity[18,27-29]. Consistent with this finding, our animal experiments showed that oral gavage of Ba significantly increased serum mannose to levels comparable to the levels achieved with 1% mannose drinking water, supporting the physiologic plausibility of a Ba–mannose axis. Future work is warranted to integrate time-resolved pharmacokinetics with intratumoral mannose quantification to define exposure–response relationships and refine translational dose optimisation.

Several limitations of the present study should be acknowledged. First, the *in vivo* studies relied on the highly immunogenic B16-F10 syngeneic melanoma model, which may not fully reflect the heterogeneity and microenvironmental

complexity of human melanoma. Whether mannose-mediated immunomodulation extends to low-immunogenicity or spontaneous tumor models remains to be determined. Second, YAP1 has context-dependent roles in T cells, including effects on proliferation, survival, and metabolic adaptation. Although live Ba is generally well-tolerated, clinical use may warrant caution in some high-risk settings, including severe immunosuppression or compromised gut barrier integrity. In addition, differences between mice and humans in immune regulation, microbiome architecture, and metabolite disposition underscore the need for further clinical studies to validate the therapeutic efficacy of Ba and mannose. In conclusion, the current study elucidated a previously unrecognized mechanism by which Ba enhances anti-tumor immunity through secretion of mannose, which suppresses YAP1 expression in $CD8^+$ T cells to unleash the cytotoxic potential and fosters a probiotic-friendly gut microenvironment.

Conclusions

We demonstrated that Ba suppresses melanoma progression and produces mannose to boosts the effector T cell *via* inhibiting YAP1 level. The current study not only identified a novel microbial metabolite with immunotherapeutic potential but also provided mechanistic insights into how gut microbiota-derived signals can systemically modulate antitumor immunity. These findings support the development of Ba or mannose as prophylactic or therapeutic agents against melanoma.

Grant support

This study was supported by the National Natural Science Foundation of China (Grant No. 82403246) and the Guangzhou Science and Technology Project (Grant No. 2025A04J4030).

Conflict of interest statement

No potential conflicts of interest are disclosed.

Author contributions

Conceived and designed the analysis: Qing Li, Haijun Deng.
Collected the data: Chengyi Li, Xuehua Zhang, Yichen Yang, Haotian Zeng, Yanqiang Shi, Jinjin Zhang, Lingjun Liu, Chenwei Zhu, Zhiwen Zhang, Chao Li, Xudong Wang, Xiaowu Bai.
Performed the analysis: Chengyi Li, Yichen Yang, Haotian Zeng.
Wrote the paper: Chengyi Li, Xuehua Zhang.

Data availability statement

The data that support the findings of this study are available from the corresponding author upon reasonable request.

References

1. Long GV, Swetter SM, Menzies AM, Gershenwald JE, Scolyer RA. Cutaneous melanoma. Lancet. 2023; 402: 485-502.
2. Larkin J, Chiarion-Sileni V, Gonzalez R, Grob JJ, Rutkowski P, Lao CD, et al. Five-year survival with combined nivolumab and ipilimumab in advanced melanoma. N Engl J Med. 2019; 381: 1535-46.
3. Wolchok JD, Chiarion-Sileni V, Gonzalez R, Grob JJ, Rutkowski P, Lao CD, et al. Long-term outcomes with nivolumab plus ipilimumab or nivolumab alone versus ipilimumab in patients with advanced melanoma. J Clin Oncol. 2022; 40: 127-37.
4. Binnewies M, Roberts EW, Kersten K, Chan V, Fearon DF, Merad M, et al. Understanding the tumor immune microenvironment (TIME) for effective therapy. Nat Med. 2018; 24: 541-50.
5. Chen DS, Mellman I. Elements of cancer immunity and the cancer-immune set point. Nature. 2017; 541: 321-30.
6. Zitvogel L, Daillère R, Roberti MP, Routy B, Kroemer G. Anticancer effects of the microbiome and its products. Nat Rev Microbiol. 2017; 15: 465-78.
7. Zitvogel L, Ma Y, Raoult D, Kroemer G, Gajewski TF. The microbiome in cancer immunotherapy: diagnostic tools and therapeutic strategies. Science. 2018; 359: 1366-70.
8. Gopalakrishnan V, Spencer CN, Nezi L, Reuben A, Andrews MC, Karpinets TV, et al. Gut microbiome modulates response to anti-PD-1 immunotherapy in melanoma patients. Science. 2018; 359: 97-103.
9. Matson V, Fessler J, Bao R, Chongsuwat T, Zha Y, Alegre ML, et al. The commensal microbiome is associated with anti-PD-1 efficacy in metastatic melanoma patients. Science. 2018; 359: 104-8.
10. Sivan A, Corrales L, Hubert N, Williams JB, Aquino-Michaels K, Earley ZM, et al. Commensal bifidobacterium promotes antitumor immunity and facilitates anti-PD-L1 efficacy. Science. 2015; 350: 1084-9.
11. Davar D, Dzutsev AK, McCulloch JA, Rodrigues RR, Chauvin JM, Morrison RM, et al. Fecal microbiota transplant overcomes resistance to anti-PD-1 therapy in melanoma patients. Science. 2021; 371: 595-602.
12. Baruch EN, Youngster I, Ben-Betzalel G, Ortenberg R, Lahat A, Katz L, et al. Fecal microbiota transplant promotes response in immunotherapy-refractory melanoma patients. Science. 2021; 371: 602-9.
13. Nocerino R, De Filippis F, Cecere G, Marino A, Micillo M, Di Scala C, et al. The therapeutic efficacy of *Bifidobacterium animalis* subsp. *lactis* BB-12® in infant colic: a randomised, double blind,

placebo-controlled trial. Aliment Pharmacol Ther. 2020; 51: 110-20.
14. Merenstein DJ, Tan TP, Molokin A, Smith KH, Roberts RF, Shara NM, et al. Safety of *Bifidobacterium animalis* subsp. *lactis* (*B. lactis*) strain BB-12-supplemented yogurt in healthy adults on antibiotics: a phase I safety study. Gut Microbes. 2015; 6: 66-77.
15. Yang C, Zha M, Li L, Qiao J, Kwok LY, Wang D, et al. *Bifidobacterium animalis* ssp. *lactis* BX-245-fermented milk alleviates tumor burden in mice with colorectal cancer. J Dairy Sci. 2025; 108: 1211-26.
16. Song Q, Li X, Li Q, Shang S, Ma S, Zhai Z, et al. *Bifidobacterium animalis* suppresses non-small cell lung cancer progression and modulates tumor immunity through indole-3-acetic acid. Cell Rep. 2025; 44: 116132.
17. Li Q, Chan H, Liu WX, Liu CA, Zhou Y, Huang D, et al. Carnobacterium maltaromaticum boosts intestinal vitamin D production to suppress colorectal cancer in female mice. Cancer Cell. 2023; 41: 1450-65.e8.
18. Kim HS, Nam JS. The multifaceted role of YAP in the tumor microenvironment and its therapeutic implications in cancer. Exp Mol Med. 2025; 57: 2201-13.
19. Li Q, Hu W, Liu WX, Zhao LY, Huang D, Liu XD, et al. *Streptococcus thermophilus* inhibits colorectal tumorigenesis through secreting β-galactosidase. Gastroenterology. 2021; 160: 1179-93.e14.
20. Rodríguez P, Rivas CI, Godoy A, Villanueva M, Fischbarg J, Vera JC, et al. Redefining the facilitated transport of mannose in human cells: absence of a glucose-insensitive, high-affinity facilitated mannose transport system. Biochemistry. 2005; 44: 313-20.
21. Rooks MG, Garrett WS. Gut microbiota, metabolites and host immunity. Nat Rev Immunol. 2016; 16: 341-52.
22. Qiu Y, Su Y, Xie E, Cheng H, Du J, Xu Y, et al. Mannose metabolism reshapes T cell differentiation to enhance anti-tumor immunity. Cancer Cell. 2025; 43: 103-21.e8.
23. de Vasconcellos Racorti N, Martinelli M, Bustos SO, Salardani M, Camacho MF, Barcick U, et al. Mannose-6-phosphate isomerase functional status shapes a rearrangement in the proteome and degradome of mannose-treated melanoma cells. J Proteome Res. 2024; 23: 5177-92.
24. Dossou AS, Mantsch ME, Sabnis N, Berg RE, Fudala R, Lacko AG. Mannose-functionalization of reconstituted high-density lipoprotein nanoparticles improves payload delivery and enhances M2-to-M1 phenotype reprogramming of RAW 264.7 macrophages polarized by B16-F10 melanoma cells. Front Drug Deliv. 2023; 3: 1281066.
25. Zhao R, Coker OO, Wu J, Zhou Y, Zhao L, Nakatsu G, et al. Aspirin reduces colorectal tumor development in mice and gut microbes reduce its bioavailability and chemopreventive effects. Gastroenterology. 2020; 159: 969-83.e4.
26. Nagasaki J, Inozume T, Sax N, Ariyasu R, Ishikawa M, Yamashita K, et al. PD-1 blockade therapy promotes infiltration of tumor-attacking exhausted T cell clonotypes. Cell Rep. 2022; 38: 110331.
27. Gao Y, Gong Y, Lu J, Yang Y, Zhang Y, Xiong Y, et al. Dihydroartemisinin breaks the positive feedback loop of YAP1 and GLUT1-mediated aerobic glycolysis to boost the $CD8^+$ effector T cells in hepatocellular carcinoma. Biochem Pharmacol. 2024; 225: 116294.
28. Alton G, Kjaergaard S, Etchison JR, Skovby F, Freeze HH. Oral ingestion of mannose elevates blood mannose levels: a first step toward a potential therapy for carbohydrate-deficient glycoprotein syndrome type I. Biochem Mol Med. 1997; 60: 127-33.
29. Hendry SA, Farnsworth RH, Solomon B, Achen MG, Stacker SA, Fox SB. The role of the tumor vasculature in the host immune response: implications for therapeutic strategies targeting the tumor microenvironment. Front Immunol. 2016; 7: 621.

Cite this article as: Li C, Zhang X, Yang Y, Zeng H, Shi Y, Zhang J, et al. *Bifidobacterium animalis* suppresses melanoma progression and activates anti-tumor immunity by inhibiting YAP1 expression in $CD8^+$ T cells. Cancer Biol Med. 2026; 23: 737-754. doi: 10.20892/j.issn.2095-3941.2025.0652